Numerical investigation of the influence of cross-sectional shape and corrosion damage on failure mechanisms of RC bridge piers under earthquake loading

Ebrahim Afsar Dizaj[a*], Mohammad M Kashani[b]

[a]Assistant Professor, Department of Civil Engineering, Azarbaijan Shahid Madani University, Tabriz, Iran. (corresponding author), Email: ebrahim.afsardizaj@azaruniv.ac.ir

Address: Iran, Tabriz, Azarbaijan Shahid Madani University, Faculty of Engineering, Department of Civil Engineering

Phone number: +989141581825

ORCID: https://orcid.org/0000-0002-7755-9983

[b]Associate Professor, Faculty of Engineering and Physical Sciences, University of Southampton, Southampton, SO17 1BJ, United Kingdom, Email: mehdi.kashani@soton.ac.uk

ORCID: https://orcid.org/0000-0003-0008-0007

Numerical investigation of the influence of cross-sectional shape and corrosion damage on failure mechanisms of RC bridge piers under earthquake loading

Ebrahim Afsar Dizaj[1], **Mohammad M Kashani**[2]

[1] Assistant Professor, Department of Civil Engineering, Azarbaijan Shahid Madani University, Tabriz, Iran. (corresponding author), Email: ebrahim.afsardizaj@azaruniv.ac.ir

[2] Associate Professor, Faculty of Engineering and Physical Sciences, University of Southampton, Southampton, SO17 1BJ, United Kingdom Email: mehdi.kashani@soton.ac.uk

Abstract

The study presented in this paper describes the coupled influence of corrosion and cross-sectional shape on failure mechanism of reinforced concrete (RC) bridge piers subject to static and dynamic earthquake loading. To this end, two RC columns varied in cross-sectional shape and corrosion degree are considered. An advanced nonlinear finite element model, which accounts for the impact of corrosion on inelastic buckling and low-cycle fatigue degradation of reinforcing bars is employed. The proposed numerical models are then subjected to a series of monotonic pushover and Incremental Dynamic Analyses (IDA). Using the analyses results, the failure mechanisms of the columns are compared at both material and component levels. Furthermore, using an existing model in the literature for uncorroded columns, a dimensionless corrosion dependent local damage index is developed to assess the seismic performance of the examined corroded RC columns. The proposed new damage index is validated against the nonlinear analyses results. It is concluded that the combined influence of corrosion damage and cross-sectional shape result in multiple failure mechanisms in corroded RC columns.

Keywords: Corrosion; Reinforced Concrete; Bridge pier; Buckling; Incremental dynamic analysis; Damage index

1. Introduction

In the last two decades, the concern of ageing and environmental deterioration of Reinforced Concrete (RC) infrastructure has increased significantly across the globe. In particular, RC bridges located in coastal environment and/or those exposed to de-icing salts are remarkably susceptible to degradation of their structural performance due to corrosion of reinforcing bars (Bertolini et al. 2004; Guo et al. 2015a). It is reported that significant percentage of RC bridges located in seismic zones of the United States are close to the end of their service life (Ghosh and Padgett 2010). The maintenance and rehabilitation of such structures need an effective tool to evaluate the time-dependent structural performance and quantify the extent of structural damage. Additionally, the aggressive agents coupled with earthquake loading result in undesired degradation mechanisms in corroded structures (Ghosh and Sood 2016). Therefore, seismic performance evaluation of corroded structures and bridges have received considerable attention in the recent years (Yuan et al. 2017; Ni Choine et al. 2016).

A number of experimental and numerical studies have been conducted to investigate the influence of corrosion on structural performance of corroded structures (Meda et al. 2014; Guo et al. 2015b; Ma et al. 2012; Alipour et al. 2011; Rao et al. 2016). The outcomes of these studies showed that corrosion affects the mechanical properties, low-cycle fatigue life, and inelastic buckling behaviour of reinforcing bars (Du et al. 2005a; Kashani et al. 2015a), and weakens the bond strength between steel and concrete interface (Fang et al. 2006). It has also been observed that the evolution of expansive corrosion products around the reinforcing bars results in detachment and delamination of concrete cover (Williamson and Clark 2000). As a result, corrosion decreases the load bearing capacity and ductility of the corroded RC components, and affects the failure mechanisms of RC components; detailed discussion is available in (Dizaj et al. 2018a). Furthermore, Kashani et al. (2019) reports a recent state-of-the-art review of the residual capacity of corroded RC components, which discusses the impact of corrosion on structural performance of RC components in detail.

Numerous modelling techniques are available in the literature to account for the impact of corrosion on structural performance of corroded RC structures. Most of these models are simply based on the reduced cross-sectional area of corroded bars (Alipour et al. 2011; Rao et al. 2016). More recently, Kashani (2014) and Dizaj et al. (2018a) developed nonlinear finite element models to simulate the nonlinear behaviour of circular and rectangular RC columns considering the effect of corrosion on inelastic buckling and low-cycle fatigue degradation of corroded bars.

In seismic vulnerability analyses of structures, the structural damage is generally quantified using a specific damage index. Although there are variety of damage indices in the literature for pristine RC structures (Cosenza and Manfredi 2000; Mergos and Kappos 2010; Schneider et al. 2015), none of them account for the adverse influence of corrosion. Akiyama et al. (2011) investigated the coupled influence of seismic hazard and airborne chloride on seismic reliability of RC bridge piers. In this study, failure probability of corroded bridge piers is estimated considering the buckling of longitudinal reinforcements as the sole damage limit state. In another study, considering the spatial steel corrosion distribution, Thanapol et al. (2016) studied seismic reliability of RC structures in marine environments. However, the outcome of previous study conducted by Dizaj et al. (2018a, 2018b) showed that seismic fragility analysis of corroded RC structures requires time-dependent (i.e. corrosion-dependent) damage indices.

Rectangular and circular cross sections are the typical cross-sectional shapes used in construction of RC structures and bridges. In the same condition of loading direction and flexural rigidity, differences in geometrical shape and arrangement of the reinforcing bars within these two cross-sectional shapes, result in a varied distribution of stresses and strains in longitudinal bars and concrete fibres. For example, the extreme tensile and compressive bars in the circular sections sustain greater strain in comparison to those of rectangular section. This will lead to its earlier yielding, fracture and/or fracture due to low-cycle fatigue failure in tension, and premature inelastic buckling followed by core concrete crushing under cyclic loading. Such differences in geometrical details of the sections may affect the failure mechanism of RC components, and hence seismic fragility of such structures will be affected. Furthermore, the previous study by Dizaj et al. (2018a) shows that corrosion of reinforcing bars changes the failure mechanism of the RC columns. However, there is no study in the literature to investigate the combined influence of corrosion damage and cross-sectional shape on failure mechanism of RC columns under dynamic earthquake loading.

Accordingly, the main contribution and novelty of the current study in comparison to preceding studies are: (*i*) constructing a dimensionless corrosion-dependent local damage index, which can be used in seismic fragility analysis of corroded RC structures, and (*ii*) investigation of the coupled influence of corrosion damage and cross-sectional shape on damage sequences and failure mechanisms of RC bridge piers. To this end, the dimensionless combined local damage index proposed by Mergos and Kappos (Mergos and Kappos 2013) is employed and modified to incorporate the influence of corrosion on damage estimation of corroded RC structures. The advantage of this damage index is accounting for multiple sources of damage including flexural deformation, shear deformation, and slippage of reinforcing bars at joint interfaces. The full description of the proposed damage index is presented in detail in the section 3 of this paper. The adequacy of the proposed damage index in failure prediction of the corroded RC columns is demonstrated in section 6 of this paper. The analyses results show that the proposed damage index is a good quantitative measure to assess the vulnerability of corroded structures. It should be noted that, since the focus of this paper is to develop a damage index to account for various failure mechanisms; it is assumed that reinforcement are uniformly corroded within the cross section and over the column height. Considering unsymmetrical corrosion scenario due to two-dimensional chloride penetration is out of the scope of this paper. Currently, there is no experimental data to quantify the impact of two-dimensional chloride penetration on unsymmetrical corrosion within the column cross section, which is an important area for future research. The influence of spatial variability of pitting corrosion over the whole length of structures is investigated in another study, and detailed discussion is available in Dizaj et al. (2018b). To this end, two identical RC columns varied in corrosion damage and cross-sectional shape (circular and rectangular section) are considered. The details of the columns are illustrated in section 2 of this paper. The failure mechanisms of the considered columns are evaluated through a series of nonlinear static and dynamic analyses. Results show that the cross-sectional shape and corrosion damage result in multiple failure mechanism in the examined RC columns. For instance, it is found that the failure of 5% corroded circular column is governed by core concrete crushing followed by premature fracture of reinforcing bars due to fatigue failure, however, the failure of the corresponding rectangular column with the same corrosion damage is governed by core concrete crushing.

2. Description of the finite element model of examined RC bridge piers

2.1 Examined RC bridge piers

To investigate the influence of cross-sectional shape on failure mechanism of corroded RC columns, a circular and rectangular cantilever RC columns are considered. For circular column, column 415 from Lehman et al. (2004) is selected from the UW–PEER experimental test database (Berry et al. 2004), and used as a benchmark. A hypothetical rectangular column is chosen such that it has the same geometrical and material properties, and fundamental period as the circular column. Both of the examined columns are flexural dominant columns. The details of examined RC columns are shown in Fig. 1 and summarised in Table 1. It should be noted that in Table 1, the effective buckling length of the vertcal reinforicng bars (L_{eff}) is calculated using the procedure proposed by Dhakal-Maekawa (Dhakal and Maekawa 2002; Kashani et al. 2016) (further details are available in Kashani et al. 2016, 2017, 2018), which has been validated against the observed experiemntal results. The mechanical properties of longitudinal and transeverse reinforcing bars are tabulated in Table 2. The compressive strength of concrete is 31 MPa.

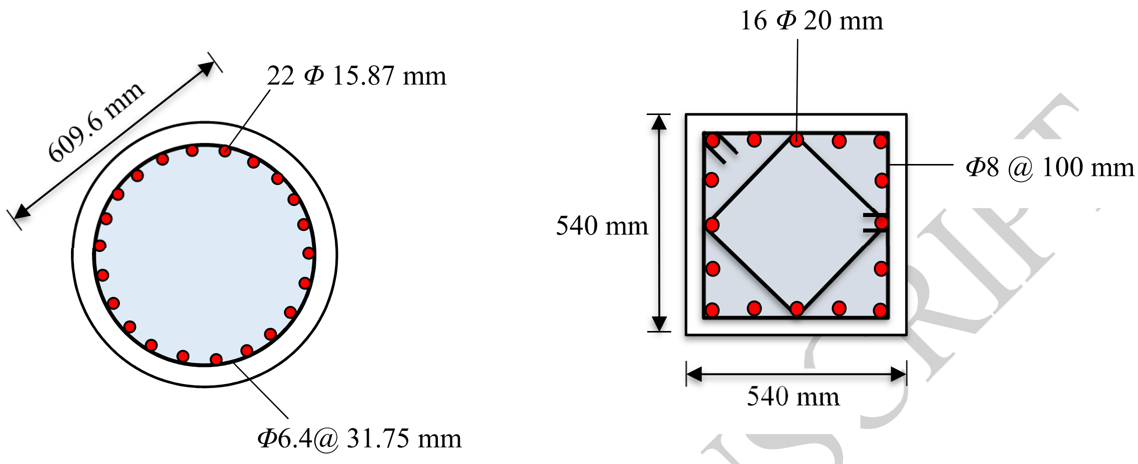

(a) (b)

Fig. 1. Cross-sectional details of the considered RC columns: a) circular column and b) rectangular column

Table 1. Details of the considered columns

Cross-sectional shape	L (mm)	L/D	L_{eff}/d	ρ_l (%)	ρ_h (%)	$N_u/(f_c A_g)$	K (N/mm)	T (sec)
Circular	2438.4	4	10	1.49	0.7	0.07	39802	0.254
Rectangular	2438.4	4.5	10	1.72	0.8	0.07	40784	0.257

Column height (L), shear span to depth ratio (L/D), the ratio of effetive buckling length of longitudinal bar to its diameter (L_{eff}/d), the longitudinal bars ratio (ρ_l), volumetric ratio of transvere reinforcements (ρ_s), axial force ratio ($N_u/f_c A_g$), un-cracked stiffness (K) and fundamental period of each column (T).

Table 2. Mechanical properties of reinforcing bars

Bar type		Transverse bars	Longitudinal bars
Yield strain	ε_y	0.0028	0.00236
Yield stress (MPa)	f_y	497	497
Elastic modulus (MPa)	E_s	210000	210000
Strain at maximum stress	ε_u	0.05660	0.13
Maximum stress (MPa)	f_u	645	662
Fracture strain	ε_r	0.16	0.195

To simulate the structural response of the RC columns, OpenSees (McKenna 2011), the open source finite element software framework, is used. To this end, the previously developed modelling technique using nonlinear fibre beam-column element by Dizaj et al. (2018a) and Kashani et al. (2016) are employed here to simulate the nonlinear response of the examined RC columns.

To simulate the nonlinear behaviour of the circular column, the nonlinear fibre beam-column element developed by Kashani et al. (2014, 2016) is used. The model comprises two force-based nonlinear fibre beam-columns elements, and each element consists of several fibre sections (known as integration points) along their length. In this model, the length of the first element is adjusted so that the integration length of first integration point (at the base of column) to be equal to the effective buckling length of the vertical reinforcement. This modelling technique is verified against an extensive set of experimental test results (further details are available in (2014, 2016)). Both the numerical models account for the impact of corrosion on combined effects of inelastic buckling and low-cycle fatigue degradation of corroded reinforcing bars.

2.2 Description of the uniaxial material models

2.2.1 Reinforcing bars

In this study the uniaxial hysteretic material model developed by Kashani et al. (2015b) is used to model the nonlinear stress-strain behaviour of corroded and uncorroded reinforcing bars. Using empirical equations, this model accounts for the effects of corrosion on the mechanical properties of reinforcing bars in tension including yield strength, ultimate strength and fracture strain, as well as inelastic buckling in compression (Du et al. 2005a, 2005b). This model is also able to simulate the simultaneous effect of corrosion on pinching response of the corroded reinforcing bars due to inelastic buckling in compression and low-cycle fatigue degradation under cyclic loading. Fig. 2 compares the backbone curve of uncorroded and corroded reinforcing steel model (with 20% of mass loss) in tension and compression (including buckling effect).

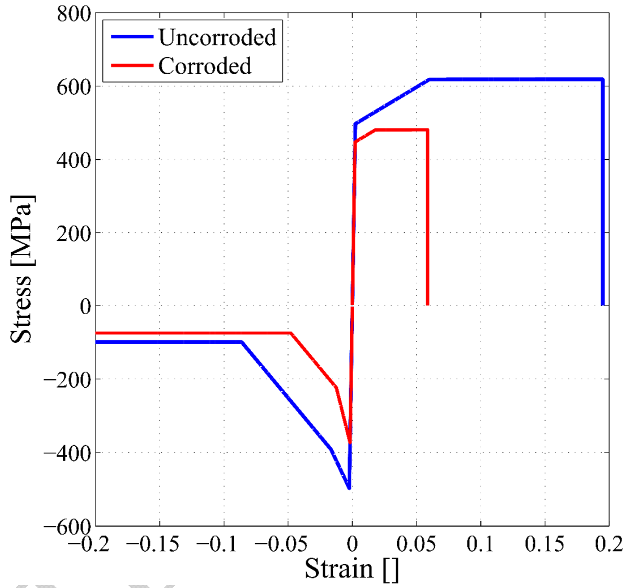

Fig. 2. Considered material model envelop for steel reinforcements

To capture the low-cycle fatigue degradation of reinforcing bars, the *Fatigue* material available in OpenSees is wrapped to the hysteretic material model. The uniaxial *Fatigue* model uses Coffin-Manson (1965) proposed relationship to account for the fatigue damage (Eq. (1)).

$$\varepsilon_p = \varepsilon_f (2N_f)^{-\alpha} \quad (1)$$

Where ε_p is amplitude of plastic strain, $2N_f$ is number of half cycles to failure and ε_f and α are material constants. Based on the experimental and analytical study conducted by Kashani et al. (2015c), the material constants ε_f and α are calibrated and are chosen to be 0.192 and -0.602 respectively. These coefficients will account for the influence of inelastic buckling on low-cycle fatigue life of reinforcing bars. Moreover, to account for the impact of corrosion on fatigue failure of reinforcements the fatigue material constants are modified using the analytical equations provided in (Kashani et al. 2015b). It should be noted that the strain localisation problem has been previously addressed in the proposed modelling technique. This has been elaborated in Kashani et al. (2016) and Dizaj et al. (2018a); where the numerical model of uncorroded and corroded bridge pier has been developed and verified against experimental data. Furthermore, the interaction between concrete cover and steel reinforcement has been taken into account in the phenomenological model of reinforcing bars. Further details are available in Kashani et al. (2016).

2.2.2 Confined and unconfined concrete

The nonlinear behaviour of confined and unconfined concrete in circular column is modelled using the uniaxial material Concrete04. To simulate the compressive stress-strain response, this constitutive material model employs the Popovics model (Popovics 1988) with linear loading and unloading degradation according to (Karsan and Jirsa 1969) and exponential decay for tensile strength. The influence of confinement on compressive strength of the confined core concrete is considered using the Mander et al. (1988) model.

The numerical simulation and comparison with experimental data by Kashani et al. (2018) showed that Mander's model (Mander et al. 1988) is not suitable for rectangular/square columns. Therefore, Concrete02 uniaxial material model, available in OpenSees, is employed to simulate the nonlinear behaviour of confined and unconfined concrete in the column with rectangular section. In compression, this model comprises a parabolic curve up to the peak and linear softening up to the residual strength which is 20% of the maximum compressive strength. In tension, this material model employs a bilinear curve, from zero to peak and from peak to zero. The effect of transverse reinforcements on stress-strain law of confined core concrete is modelled using the modified Kent-Park model (Scott et al. 1982).

In the proposed numerical model, the corrosion induced concrete cover cracking/spalling is considered through reduction of its compressive strength. Here, to account for the impact of corrosion on stress-strain behaviour of concrete cover, the compressive strength and its corresponding strain is reduced using the technique proposed in Coronelly and Gambarova (2004). The impact of corrosion on stress-strain behaviour of the confined core concrete is also considered using the approach proposed (Kashani 2014). This simplified approach has been validated against benchmark experimental data (Dizaj et al. 2018a). According to this approach, first the mechanical properties of confinement is modified using the following equations (Du et al. 2005a, 2005b):

$$f_{yh,corr} = (1 - 0.005\psi_h) f_{yh} \tag{2}$$

$$\rho_{s,corr} = (1 - 0.01\psi_h)\, \rho_s \tag{3}$$

where $f_{yh,corr}$, f_{yh}, $\rho_{s,corr}$, ρ_s and ψ_h are yield strength of corroded hoops, yield strength of sound hoops, volumetric ratio of corroded hoops, volumetric ratio of sound hoops and mass loss percentage of hoops, respectively. Then, using the modified Kent and Park model (Scott et al. 1982) the compressive strength of unconfined concrete (f_c) in rectangular column is multiplied by K_c factor according to Eq (4):

$$K_c = 1 + \frac{f_{yh}\rho_s}{f_c} \tag{4}$$

As mentioned above, for circular column, Mander's model (Mander et al. 1988) is used to modify the compressive strength of confined core concrete instead of Eq (4). Fig. 3 compares the compressive stress-strain behaviour of confined concrete for uncorroded and corroded (with 20% of mass loss) rectangular columns. The ultimate compressive strain of confined core concrete is calculated based on the approach proposed by Priestley and Paulay (1992). Here, using a simple procedure, th effects of corrosion on ultimate compressive strain of confined core concrete is considered. Further details are provided below the Eq (9).

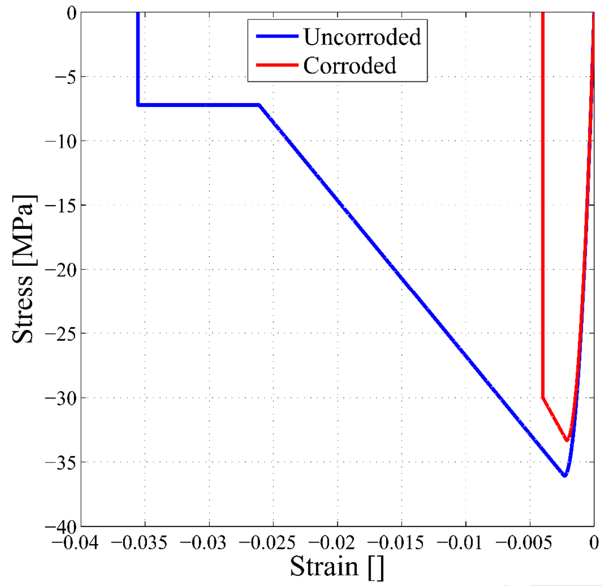

Fig. 3. Considered envelop for compressive behaviour of confined core concrete

2.2.3 Bar-Slip model

The slippage of reinforcing bars at joint interfaces (column footing, beam-column connection, etc.) of RC components due to strain penetration results in fixed-end rotation which is one of the primary sources of damage in RC structures (Mergos and Kappos 2015). To accurately model the lateral stiffness of RC structures, the fixed-end rotations should be considered in numerical model. In the present study, the stress-slip constitutive material model developed by Zhao and Sritharan (2007) is assigned to a zero-length section element at the base of the columns. It should be noted that since the anchorage zone in column base is in an enough depth to be survive from aggressive agents, it is assumed that reinforcing bars are not corroded at below the foundation and hence, uncorroded bar-slip model is used in all the analyses. Further details are available in (2018a).

3. Description of the proposed local damage indices

The vulnerability of structures against seismic loading is generally assessed in terms of a seismic damage limit state. The damage limit state should be linked to a physical definition, which is normally in a form of a damage index between zero and unity, representing from no damage to collapse. A wide range of local and global damage indices are proposed by different researchers (Rodriguez 2015; Kappos 1997). Most of the previously proposed damage indices are based on the flexural damage, while contribution of other sources of damage like shear deformation and slippage of longitudinal reinforcements are ignored (Mergos and Kappos 2013).

Mergos and Kappos (2013) developed a combined local damage index for seismic assessment of RC structures, which incorporates the contribution of all deformation mechanisms including flexural, shear, and slippage of reinforcements. This damage index is described in the Eqs. (5-8):

$$\lambda_{tot}=1-\left(1-D_{fl}\right).\left(1-D_{sh}\right).\left(1-D_{sl}\right) \tag{5}$$

$$D_{fl}=\left(\frac{\varphi_{\max}-\varphi_0}{\varphi_u-\varphi_0}\right)^{\lambda_{fl}} \tag{6}$$

$$D_{sh}=\left(\frac{\gamma_{\max}-\gamma_0}{\gamma_u-\gamma_0}\right)^{\lambda_{sh}} \tag{7}$$

$$D_{sl}=\left(\frac{\theta_{sl,\max}-\theta_{sl,0}}{\theta_{sl,u}-\theta_{sl,0}}\right)^{\lambda_{sl}} \tag{8}$$

where, λ_{tot} is the total damage index, and D_{fl}, D_{sh} and D_{sl} are the contribution of flexural, shear damage and reinforcement slippage damage, respectively; λ_{fl}, λ_{sh} and λ_{sl} are exponents representing the rate of flexural damage, shear damage and bond slip damage progression, respectively. Furthermore, φ_{max}, γ_{max} and θ_{max} are maximum curvature, maximum shear strain and maximum fixed-end rotation caused by slippage of reinforcement, respectively; φ_0, γ_0 and $\theta_{sl,0}$ are associated threshold values of flexural damage, shear damage and bond-slip damage, respectively. φ_u, γ_u and $\theta_{s,u}$ are the ultimate values of deformation capacities based on the monotonic pushover analysis (Mergos and Kappos 2013). Based on the experimental calibrations conducted by Mergos and Kappos (2013), the values of λ_{fl}, λ_{sh} and λ_{sl} are proposed to be 1.35, 0.8 and 0.95, respectively. Moreover, for simplification, the values of φ_0, γ_0 and $\theta_{sl,0}$ are assumed to be zero (Mergos and Kappos 2013). The advantage of this damage index is that once each of damage indices reaches to the unity, immediately total damage index become 1, indicating the failure of structure. Further details about this damage index is available in (Mergos and Kappos 2013).

In this paper the efficiency of this damage index in seismic performance assessment of examined corroded RC bridge piers is evaluated through a series of Incremental Dynamic Analyses (IDAs). To this end, Φ_u, γ_u and $\theta_{s,u}$ are modified to account for the impact of corrosion on various failure modes of corroded columns. Further details are provided in the next section.

3.1 Influence of corrosion on ultimate deformation capacities

Seismic vulnerability analysis of corroded RC structures has received a considerable attention during the past decade (Ghosh and Padgett 2010; Ghosh and Sood 2016). In most of the previous studies, the level of damage is quantified using the global time-invariant damage limit states like drift ratio (Guo et al. 2015; Alipour et al. 2011). However, recent study conducted by Dizaj et al. (2018a), demonstrated that time-invariant damage limit states are not suitable for corroded structures, and do not realistically represent the onset of failure of corroded structures (Dizaj et al. 2018a). It should be noted that corrosion is a time-variant phenomenon, and therefore, damage limit states that accounts for corrosion are time-variant limit states. The considered damage limit states are: (*i*) Associated drift with yielding of longitudinal bars, (*ii*) Associated drift with spalling of concrete cover, and (*iii*) Associated drift with crushing of concrete core. All of this three criterions are mass loss dependent, and mass loss is a function of time. Therefore the considered damage limit states are indirectly time-dependent. The proposed time-dependent damage limit states have been described in detail in Dizaj et al. (2018b).

In this study the local damage index proposed in (Mergos and Kappos 2013) is modified to account for the influence of corrosion. To generate the data for modification of the uncorroded local damage indices, nonlinear finite element analysis is employed as follows.

3.1.1 Influence of corrosion on flexural damage index, φ_u

The curvature capacity φ_u, is considered as the minimum of the corresponding curvature to the three different damage criterions including: (*i*) core concrete crushing; (*ii*) fracture of tensile reinforcing bars and (*iii*) 20% maximum moment capacity loss. The corrosion-damaged core concrete crushing strain, ε_{cu} which is corresponding to fracture of first spiral/hoop reinforcement described in Eq. (9) (Priestley and Paulay 1992):

$$\varepsilon_{cu} = 0.004 + 1.4\left[\frac{\rho_{s,corr} f_{yh,corr}\, \varepsilon_{uh,corr}}{f_{cc,corr}}\right] \tag{9}$$

where $\rho_{s,corr}$, $f_{yh,corr}$, $\varepsilon_{uh,corr}$ are volumetric ratio, yield strength and strain corresponding to ultimate stress of corroded transverse reinforcements and $f_{cc,corr}$ is compressive strength of core concrete considering the impact of corrosion on confinement. All the parameters are a function of percentage of mass loss and modified according to the approach presented in (Dizaj et al. 2018a). Fracture strain of corroded tensile reinforcing bars, ε_u, is obtained using the empirical Eq. (10), which is proposed by Du et al. (2015b) and validated in modelling corroded RC columns by Dizaj et al. (2018a).

$$\varepsilon_u = \left(1 - 0.035\psi\right)\varepsilon_{ul} \tag{10}$$

where ψ is the percentage mass loss, and ε_{ul} is the fracture strain of uncorroded reinforcement.

3.1.2 Influence of corrosion on shear damage index, γ_u

The shear strain corresponding to onset of shear failure, γ_u, is calculated using the Eq. (11) (Mergos and Kappos 2013):

$$\gamma_u = \lambda_1.\lambda_2.\lambda_3.\gamma_{st} \geq \gamma_{st} \tag{11}$$

where λ_1, λ_2 and λ_3 are empirical modification factors according to (Mergos and Kappos 2013) and γ_{st} is modified shear deformation corresponding to the onset of yielding of shear reinforcement, γ_{truss}. Due to the significant paucity in literature, to investigate the impact of corrosion on shear strength of corrosion-damaged concrete and shear/transverse reinforcement, a simplified methodology is adopted to account for the corrosion of shear reinforcement. In this study, Eqs. (12-13) are used to calculate λ_3:

$$\lambda_3 = 0.31 + 17.8.\min\left(\omega_\kappa, 0.08\right) \tag{12}$$

$$\omega_\kappa = \frac{A_{h,corr} f_{yh}}{b.s.f_c} \tag{13}$$

where, $A_{h,corr}$ is the cross-sectional area of the corroded transverse reinforcements running parallel to the applied shear force according to Eq.(14), b is column width/diameter and s is spacing of the hoops/spirals.

$$A_{h,corr} = \left(1 - 0.01\psi\right) A_h \tag{14}$$

In Eq. (14), A_h is the cross-sectional area of uncorroded stirrups. Mergoes and Kappos (2013), proposed the Eq. (15) to calculate γ_{st}:

$$\gamma_{st} = \kappa.\lambda.\gamma_{truss} \tag{15}$$

where γ_{truss} is calculated from Eq. (13):

$$\gamma_{truss} = \frac{V_{st}}{GA_1} + \gamma_{cr} \tag{16}$$

where V_{st} is shear strength of transverse reinforcements and GA_1 is the post yield stiffness of V-γ skeleton curve proposed in (Mergos and Kappos 2012). Due to lack of studies about the effect of corrosion on shear strength of RC structures in the literature, V_{st} and GA_1 are calculated based on the reduced spiral/hoop bar diameter. It should be noted that the focus of this study is on flexural columns, and therefore, shear deformations are within the elastic region.

3.1.3 Influence of corrosion on slippage damage index, $\theta_{s,u}$

A zero-length section element in conjunction with a constitutive stress-slip law is used to account for the fixed-end rotation at joint interface. The ultimate fixed-end rotation capacity, $\theta_{s,u}$, is calculated using the Eq. (17):

$$\theta_{s,u} = \frac{S_u}{d - x_c} \tag{17}$$

where, d is the effective depth measured from centre of tensile reinforcement to the outmost compressive side of the section, x_c is the depth of the neutral axis and S_u is the ultimate slip which is assumed to be 30 S_y (Zhao and Sritharan 2007), where S_y is the yielding slip of reinforcing bars which is calculated using the relationship proposed in (Zhao and Sritharan 2007).

4. Monotonic and cyclic pushover analyses

Other than uncorroded columns, to evaluate the impact of corrosion on deformation capacities, three different levels of corrosion including 5% (lightly corroded structure), 10% (moderately corroded structure) and 20% (heavily corroded structure) mass losses are considered for each column type. The corrosion of tie reinforcement, however, is generally higher than the main vertical reinforcement as they are closer to the surface. The considered corrosion level of ties for abovementioned corroded structures are 12%, 24% and 42%, respectively. The corrosion of tie reinforcement is calculated using the methodology that was used in Dizaj et al. (2018a).

Fig. 4 shows the pushover analyses results of the examined RC columns. For each level of corrosion, the capacity curve of circular column is compared with that of rectangular column. Moreover, damage limit states are also mapped on each curve. Here, the spalling of the concrete cover is assumed to occur when the compressive strain of extreme fibre exceeds 0.004 (Priestley and Paulay 1992). For corroded columns, the spalling strain is a function of corrosion and is modified using the approach proposed in (Coronelli and Gambarova 2004).

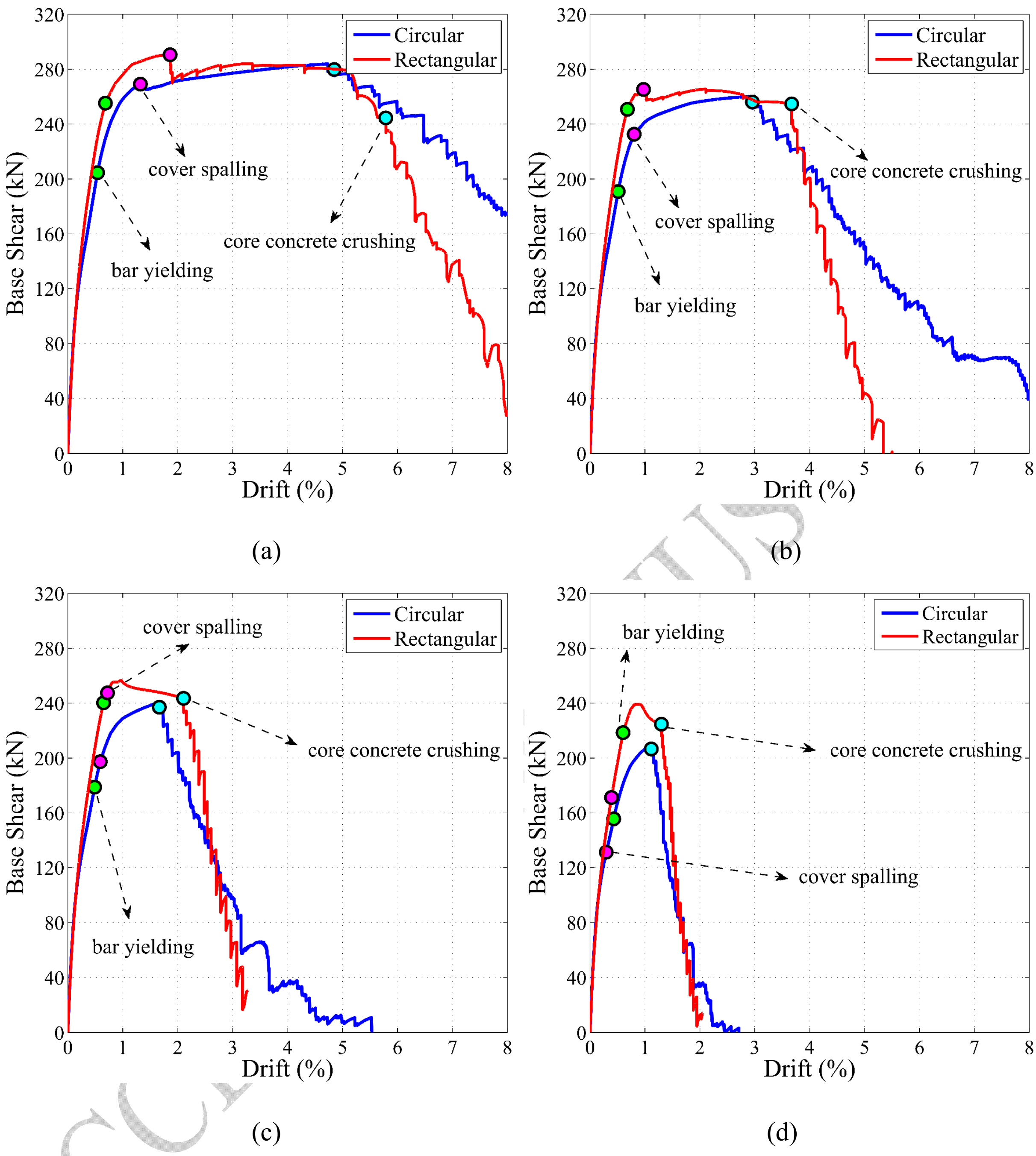

Fig. 4. Results of pushover analysis: (a) uncorroded; (b) 5% corroded; (c) 10% corroded and (d) 20% corroded columns

As it is shown in Fig. 4, in all the cases, the failure of the columns is mainly dominated by core concrete crushing. However, in circular column, the core concrete crushing happens in a slightly less drift percentage comparing to rectangular column. This is because, in empirical Eq. (9) which is used to determine the crushing strain of the core concrete, all the parameters are almost identical for both circular and rectangular sections, except the ultimate compressive strain of core concrete ($f_{cc,corr}$) which is a greater value in circular section.

As shown in Fig. 4, it is evident that as the level of corrosion increases, the flexural capacity of the columns and corresponding drift of each damage limit state decreases significantly. For example, while the corresponding drift of core crushing is approximately 5% in uncororded circular column (Fig. 4(a)), it is declined to approximately 1% in 20% corroded circular column (Fig. 4(d)).

Fig. 4(d) shows that the severe corrosion at 20% mass loss, changes the nonlinear behaviour of columns, where cover spalling takes place prior to yielding of the first vertical bar. This confirms that corrosion affects the damage limit states and structural behaviour of RC structures. Hence, to accurately assess the seismic performance of corroded RC structures the damage limit states should be considered as a function of corrosion damage.

For each column, deformation capacities and associated drifts to the damage limit states are extracted from the pushover analyses and tabulated in Table 3.

Table 3. Deformation capacities and associated drifts of damage limit states

Section shape	**ψ (%)**	**φ_u (1/m)**	**$\theta_{sl,u}$ (rad)**	γ_u	***Drift ratio at bar yielding***	***Drift ratio at cover spalling***	***Drift ratio at core concrete crushing***
Circular	0	0.220	0.036	0.038	0.005	0.013	0.048
	5	0.135	0.036	0.032	0.005	0.008	0.030
	10	0.062	0.036	0.028	0.005	0.006	0.017
	20	0.033	0.036	0.022	0.004	0.003	0.011
Rectangular	0	0.24	0.051	0.035	0.007	0.019	0.058
	5	0.155	0.051	0.030	0.007	0.010	0.037
	10	0.070	0.051	0.026	0.006	0.007	0.021
	20	0.039	0.051	0.021	0.006	0.004	0.013

Using the experimental loading history of Lehman's column 415 specimen (Lehman et al., 2004), an exemplary cyclic pushover analysis carried out on each corroded and uncorroded circular column to investigate the impact of corrosion on variation of the different damage mechanisms (flexure, shear and slip) and total damage index. Fig. 5 shows the evolution of the proposed damage index for individual damage mechanisms. Fig. 5 indicates that as corrosion level increases the column fails at lower cycle numbers.

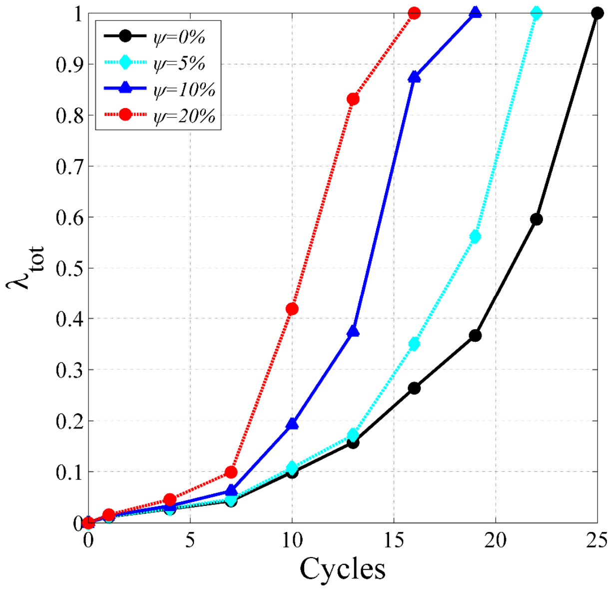

Fig. 5. Total damage index evolution of circular column in cyclic analysis

5. Incremental Dynamic Analysis (IDA)

In this part, the coupled influence of cross-sectional shape and corrosion damage on failure mechanism of the considered RC columns is investigated through IDA. To this end, 44 far-field ground motions (22 pairs) which are listed in FEMA P695 (2009) are selected. All the selected ground motion records are scaled to their corresponding spectral acceleration at fundamental period of the structure, $S_a(T_1)$. Then using the increased $S_a(T_1)$, a series of time-history analyses repeated until the structure fails. Finally, for each ground motion, the maximum absolute drift ratio (ratio of tip displacement to the column height) is plotted versus the multiples of $S_a(T_1)$ to establish the IDA curves. It should be noted that, the uncertainties in corrosion phenomenon has already been investigated in Dizaj et al. (2018b). However, based on the results of numerical simulations reported in Dizaj et al (2018b), the uncertainties associated with earthquake ground motions are much more critical than corrosion.

5.1 Discussion of the IDA results

Fig. 6 shows exemplary IDA results for each uncorroded columns. Based on the median (50% fractile) IDA curves in Fig. 6, the uncorroded rectangular column fails in a lower drift ratio in comparison with the corresponding circular column.

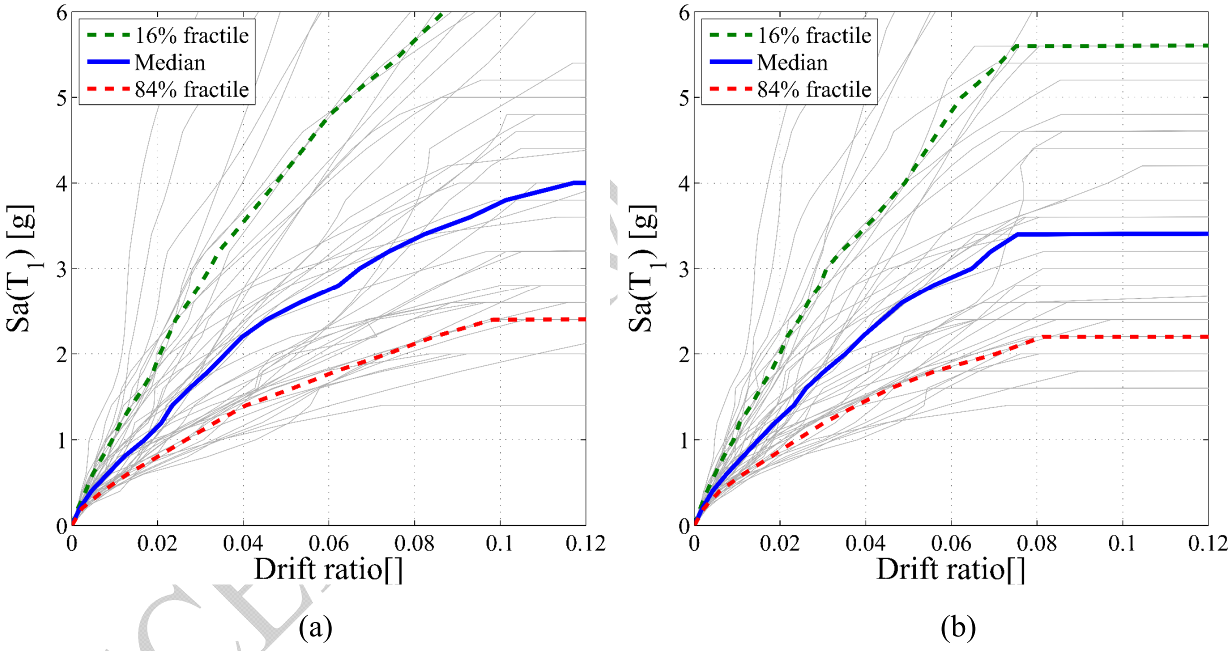

Fig. 6. IDA results: (a) uncorroded circular column; (b) uncorroded rectangular column

Fig. 7 compares the median IDA curves of circular columns with those of rectangular columns. Based on the Fig. 7, the corroded columns fail in a less drift ratio in comparison with the uncorroded columns. For example, while uncorroded rectangular column fails in approximately 0.08 drift ratio (Fig. 6(b)), its corresponding 10% corroded column fails in about 0.03 drift ratio. Moreover, it can be clearly seen that for uncorroded and 5% corroded cases while the rectangular column collapses in approximately 0.05 and

0.075 drift ratio, respectively, their corresponding circular columns exhibit a more ductile behaviour and fail in approximately 0.065 and 0.115 drift ratio, respectively. However, for higher levels of corrosion, both of the columns show similar behaviour and fail at the same drift ratio. For example, both 20% corroded columns fail in approximately drift ratio of 0.02. However, the summarised IDA curves are not a sufficient tool to make accurate judgments about the mechanism of failure as they just display the global behaviour of the considered structures. To investigate the behaviour of the columns further at the material level, material responses at the critical section (base) of the columns are recorded.

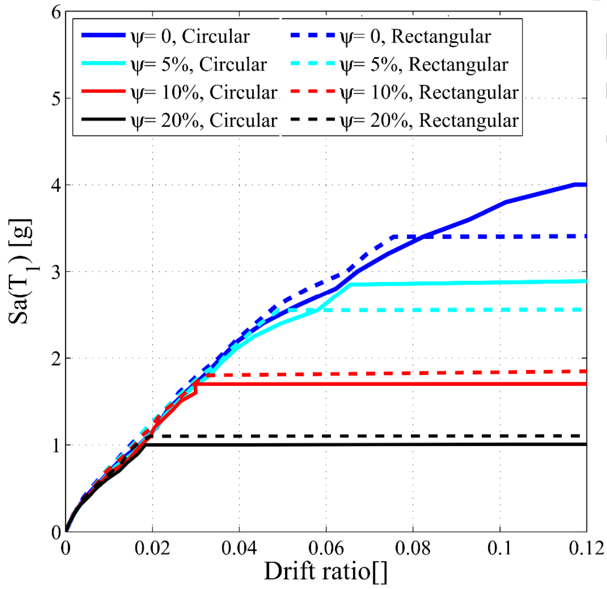

Fig. 7. Comparing median IDA results of circular columns with those of rectangular columns

Fig. 8 shows the dispersion of normalised core concrete strain (ε_c/ ε_{cu}) of each column against its corresponding drift ratio. The normalised core concrete strain is the ratio of maximum absolute value of compressive core concrete strain at each imposed intensity level of each earthquake excitation ε_c, to its ultimate value ε_{cu}.

From the Fig. 8, it can be clearly seen that as the level of corrosion increases, the onset of core concrete crushing occurs at lower drift ratios. For example, the onset of core concrete crushing of the uncorroded circular column is corresponding to drift ratio of 0.065 (Fig. 8(a)), but it is reduced to less than 0.02 for 20% corroded column (Fig .8(d)). Moreover, Fig. 8(a) indicates that the normalised concrete strains of uncorroded circular column is more scattered in comparison with those of uncorroded rectangular column. For example, beyond 0.08 drift ratio there are rare points for rectangular column. This is related to the influence of cross section geometry. In rectangular columns, once the outmost fibres of core concrete crushes in compression, the whole row of fibres in the section is crushed. Consequently, it fails rapidly and cannot experience higher drifts. This is confirmed by Fig. 6(b), where the uncorroded rectangular column is failed at approximately 0.08 drift ratio. However, the circular section can tolerate higher drift ratios because the compressive part of the section is crushing more gradually after the crushing of outmost fibres of concrete core. Furthermore, this also affects the inelastic buckling behaviour of bars in compression as well. The vertical bars in circular column buckle gradually. However, all the vertical bars on the compression side of the rectangular column buckle together. This buckling mechanism results in premature core concrete crushing in compression, and hence, brittle failure. However, Fig. 8(d) shows that beyond the 0.03 drift ratio the 20% corroded columns are collapsed while we don't see any points in this region, which is comparable with their median IDA curve presented in Fig. 5.

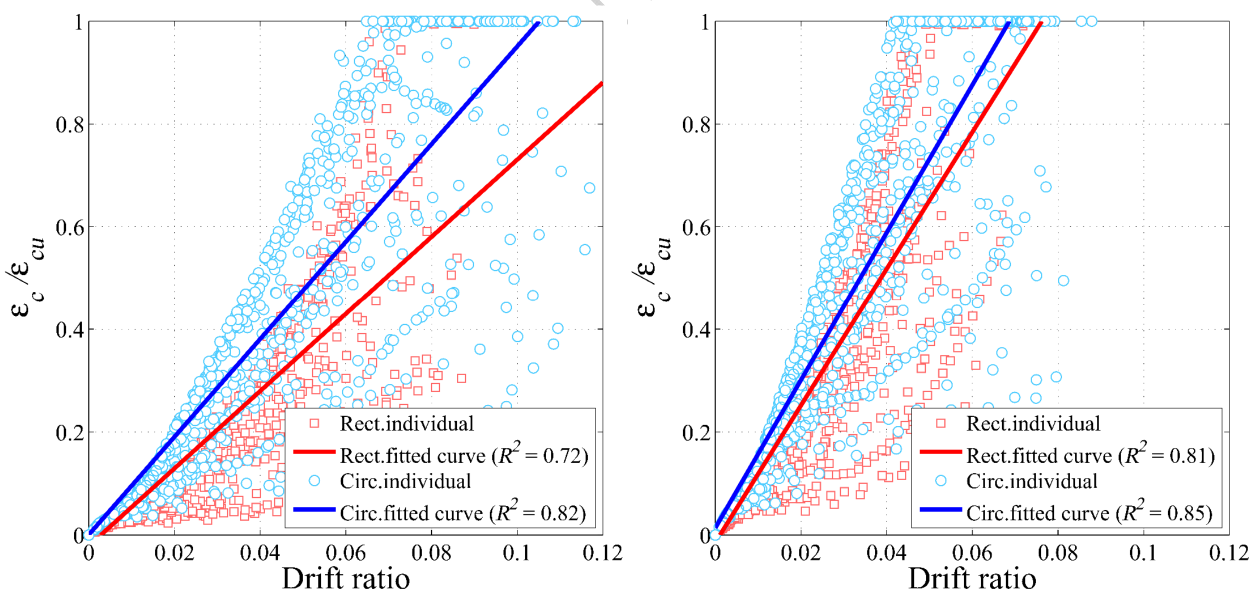

(a) (b)

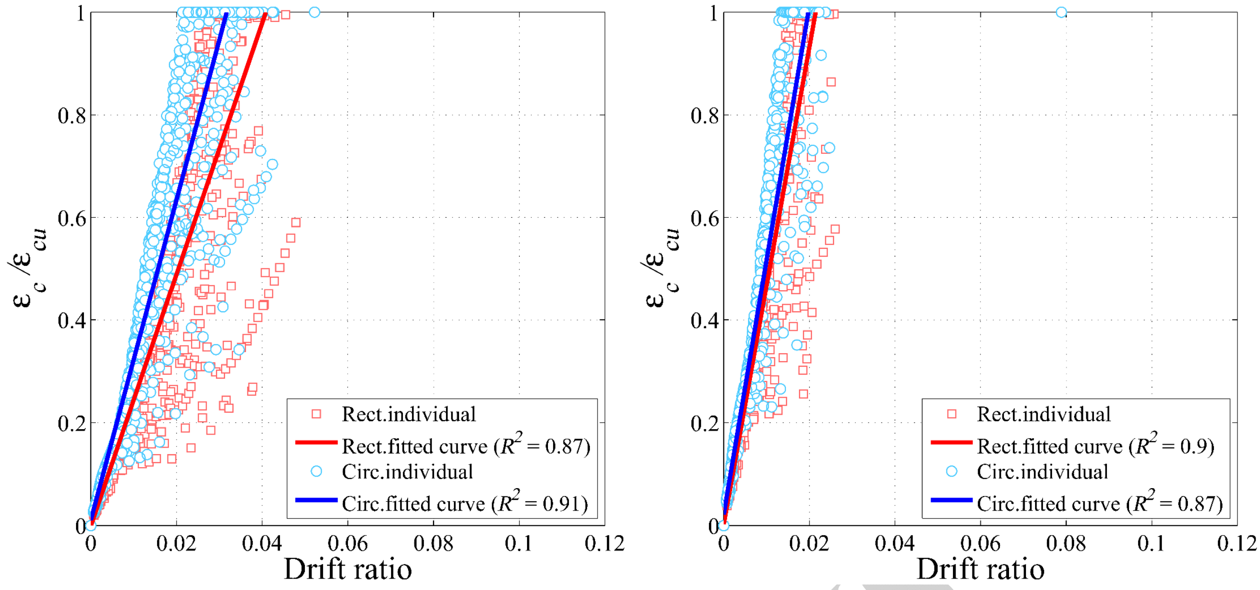

(c) (d)

Fig. 8. Dispersion of the normalised core concrete strain versus drift ratio: (a) uncorroded; (b) 5% corroded; (c) 10% corroded and (d) 20% corroded columns

Fig. 9 displays the normalised strain ratios ($\varepsilon_s / \varepsilon_u$) of the extreme longitudinal reinforcement versus its corresponding drift ratio. The normalised strain ratio of longitudinal reinforcing bars is the ratio of maximum value of tensile reinforcement strain at each applied intensity level of each earthquake ground motion record ε_s, to its ultimate corroded strain value ε_u. It is apparent from the Fig. 9(a) that up to 0.12 drift ratio, longitudinal bars are not fractured in neither of the uncorroded columns. This confirms that the failure of the uncorroded columns is governed by core concrete crushing. However, Fig 9(a) shows that the outmost tensile reinforcement in circular section undergoes higher strains than that of rectangular column. This is related to arrangement of the reinforcing bars in circular section, where there is one bar in outmost tension side of the column.

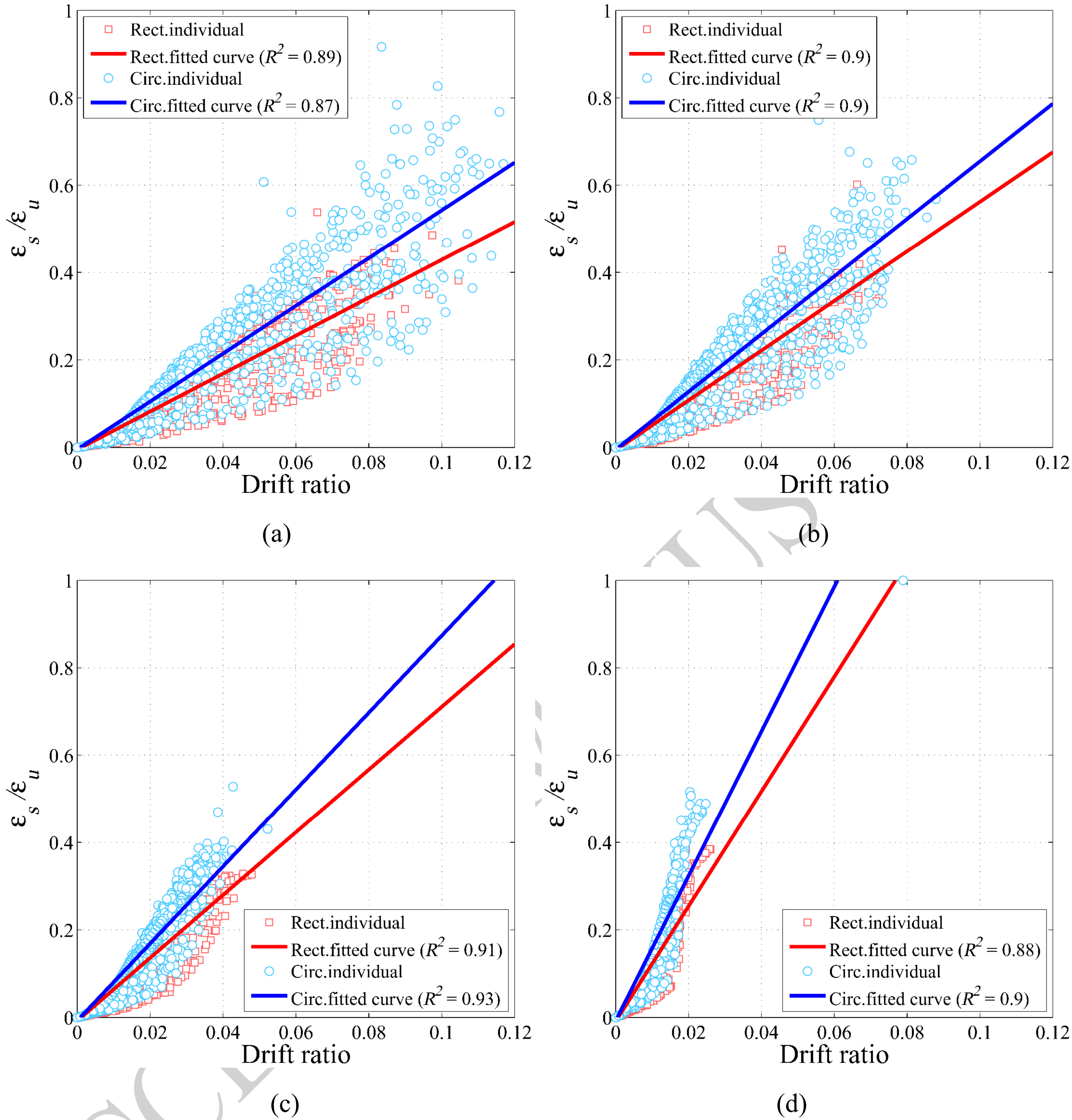

Fig. 9. Dispersion of the normalised reinforcement strain versus drift ratio: (a) uncorroded; (b) 5% corroded; (c) 10% corroded and (d) 20% corroded columns

As illustrated in Fig. 9, it can be concluded that in any of the corroded columns vertical bars have not reached to the fracture strains.

Other than crushing of core concrete and fracture of tensile reinforcement, low-cycle fatigue degradation of vertical reinforcement is also recognised as one of the important sources of failure of RC structures (Kashani et al. 2015b). In Fig. 10, the maximum value of fatigue damage index at each IDA scale factor is plotted against its corresponding drift ratio. Comparing Fig. 10 with Fig. 9, it can be concluded that in both uncorroded and 5% corroded circular columns, the low-cycle fatigue failure is preceding to fracture of reinforcement. This is while except for a couple of cases, the vertical bars of the rectangular column do not experience the fatigue failure. This is because in circular section the fatigue damage is accumulated in bars at near the top of the section. Moreover, comparing Fig. 10 with Fig .8, while in uncorroded circular column the onset of fatigue failure occurs prior to the onset of core concrete crushing, in most of the cases in 5% corroded circular column these two are happening simultaneously. However, as can be seen in Figs. 10 (c) and 8(d), as the corrosion level increases both the columns are demolished before low-cycle fatigue happens. These is because, in the higher levels of corrosion (10% and 20%), the quick fracture of confinement results in quick failure of the columns due to the core concrete crushing.

The finding of this part suggests that while according to the previous studies (Kashani et al. 2015a) corrosion declines the fatigue life of the corroded bare bars, but the extra corrosion of embedded reinforcing bars may not lead in fatigue failure due to the premature collapse of the component.

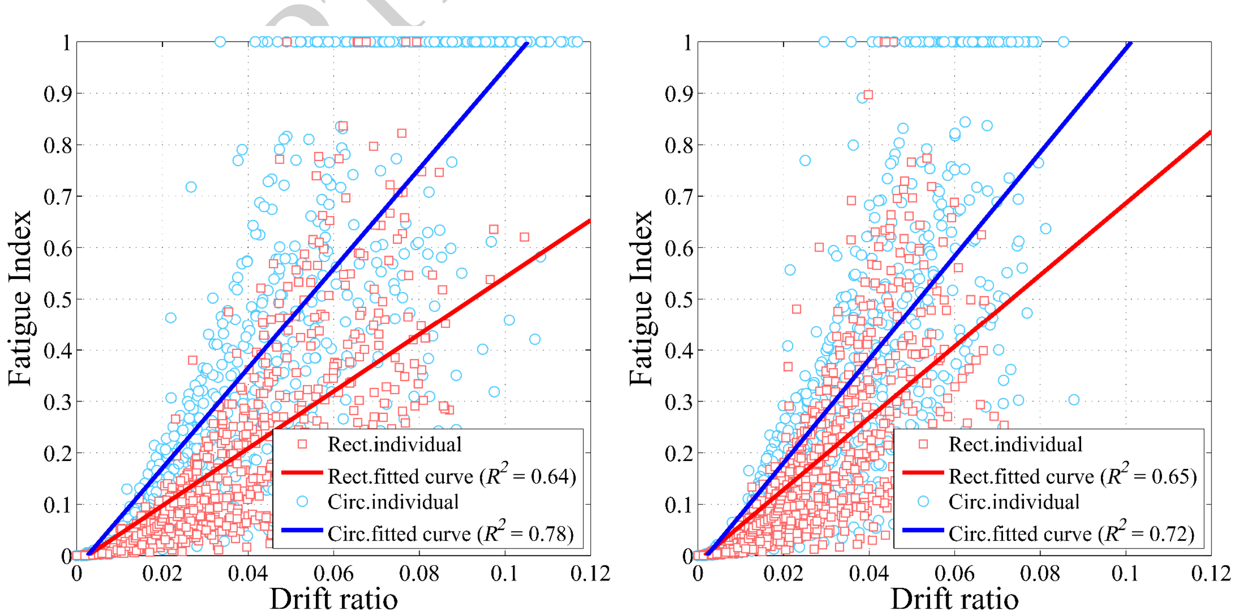

(a) (b)

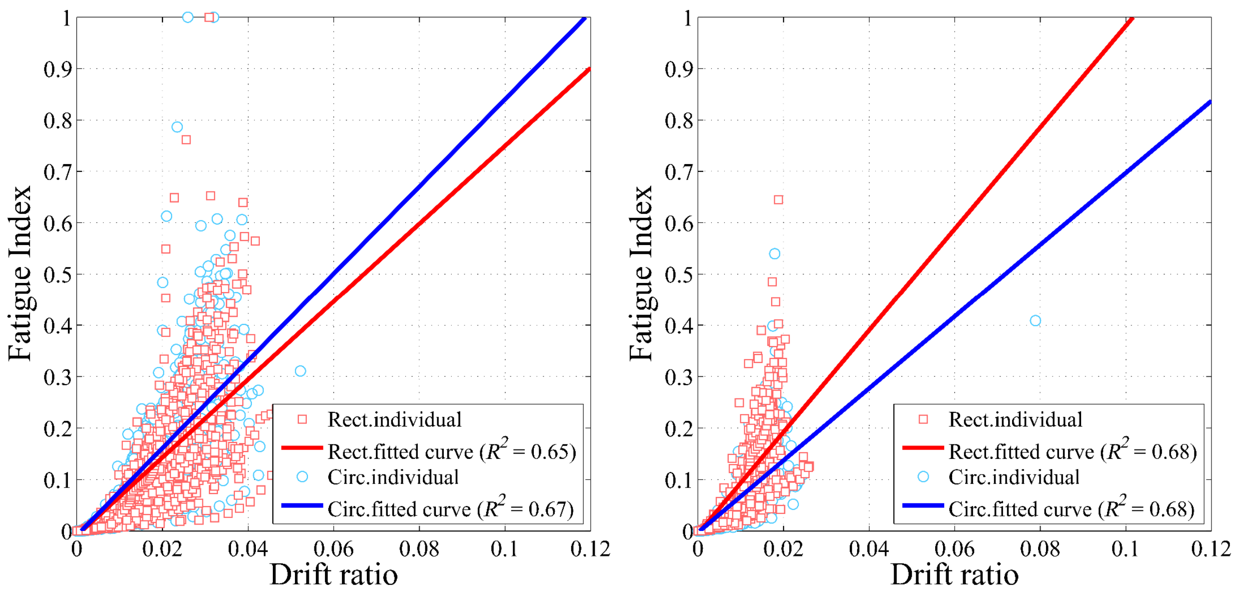

(c) (d)

Fig. 10. Dispersion of the fatigue index versus drift ratio: (a) uncorroded; (b) 5% corroded; (c) 10% corroded and (d) 20% corroded columns

6. Validating the efficiency of proposed local damage indices

The aim of this section is to investigate the adequacy of the proposed modified local damage indices on failure assessment of the corroded RC structures subjected to earthquake loading. To this end, the total damage index (λ_{tot}) is calculated using the Eq. (5) for each incremented time history analysis. Fig. 11 shows each calculated value of λ_{tot} for circular and rectangular columns against their corresponding maximum absolute value of drift ratios.

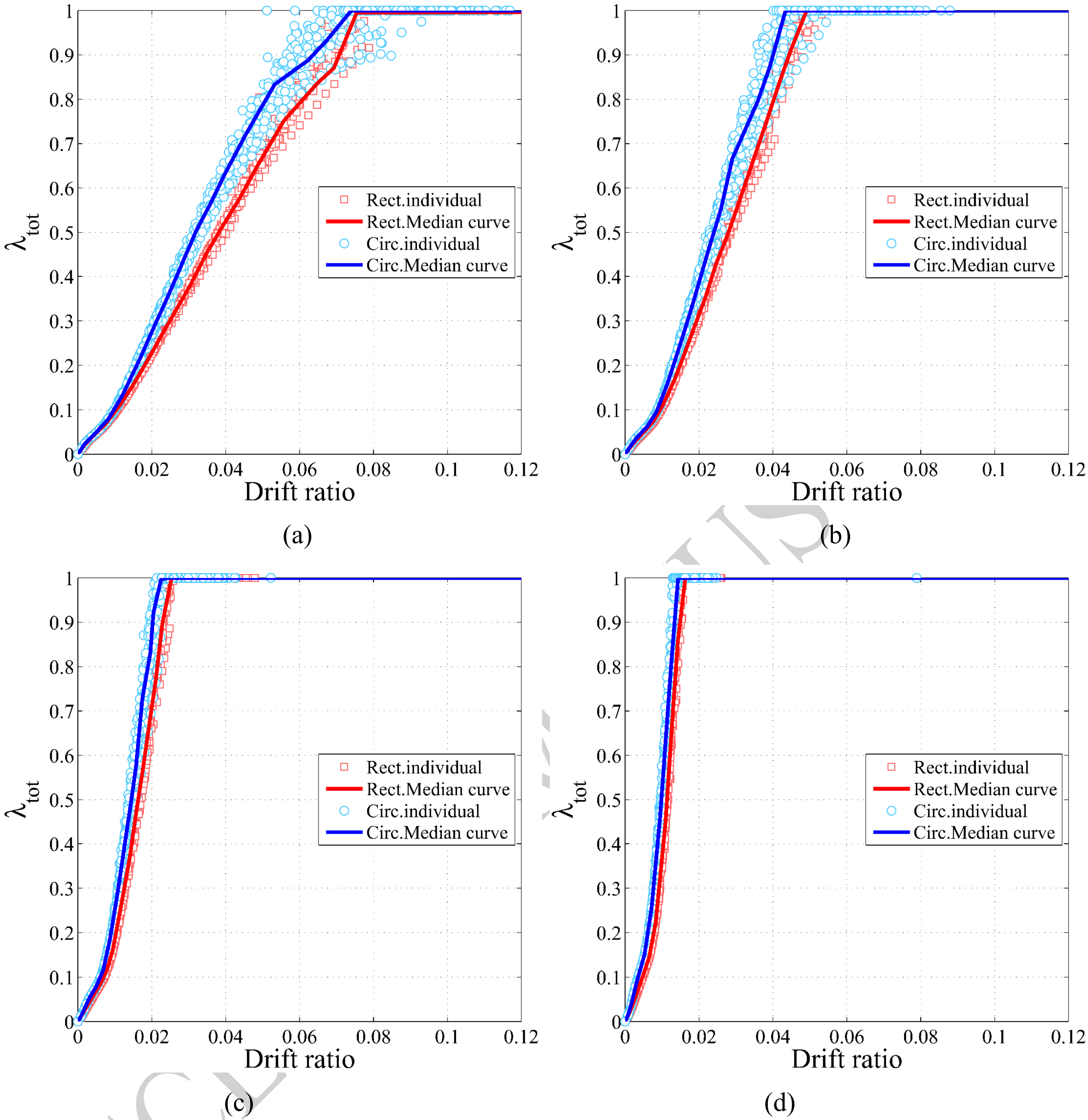

Fig. 11. Distribution of total damage index against the corresponding drift ratio: (a) uncorroded; (b) 5% corroded; (c) 10% corroded and (d) 20% corroded columns

Comparing Fig. 11 with Fig. 8, shows that in all the considered cases the onset of core concrete crushing is predicted well with the proposed damage index. For example, comparing Fig. 11(d) with Fig. 8(d), the onset of λ_{tot}=1 in 20% corroded rectangular column is corresponding to approximately 0.018 drift ratio which is almost identical to that of core concrete crushing for the same column. Regarding the failure of all the considered columns with different levels of corrosion is dominated by core concrete crushing, it can be concluded that the failure of the columns is predicted well using the proposed damage index.

In order to show the effectiveness of proposed local damage indices in failure prediction of columns, the median of drift ratios corresponding to median of the λ_{tot}=1 points are obtained for each level of corrosion from Fig. 11. Then, in Fig. 12, they are shown by vertical lines and compared with the median IDA curves. Fig. 12(a) and Fig. 12(b) show that the failure of uncorroded and 5% corroded rectangular columns are predicted precisely by the proposed damage index. Similarly, Fig. 12(c) and Fig. 12(d) indicate that the onset of failure in 10% and 20% corroded is also relatively well anticipated with the proposed damage index. However, based on the Fig. 12(a), the failure of the ucorroded circular column is estimated somewhat conservatively by the proposed damage index. This is because, as described earlier in this paper, the ultimate curvature, φ_u, is corresponding to the onset of core concrete crushing. This means that the total damage index reaches to the unity once the outmost fibres of core concrete crushes. However, as discussed in part 5.1 of this paper, due to the influence of cross section geometry, the circular column can tolerate higher deformation even after crushing of extreme fibres of core concrete. On the other hand, the shear deformation is considered to be in elastic region. In addition, the axial-flexure-shear interaction of uncorroded and corroded columns is not accounted in this model. This might be sorted out using shell or brick element modelling technique (Belletti and Vecchi, 2018; Di Carlo et al., 2017), and therefore, is an area for future research.

In summary, the proposed damage index shows a promising alternative to the conventional time-invariant damage limit states for seismic fragility analysis of corroded structures. However, there is need for further experimental and parametric study using numerical models to improve this damage index to account for the axial-shear-flexure interaction. Nevertheless, this paper creates and avenue for other researchers to continue this work in the future research.

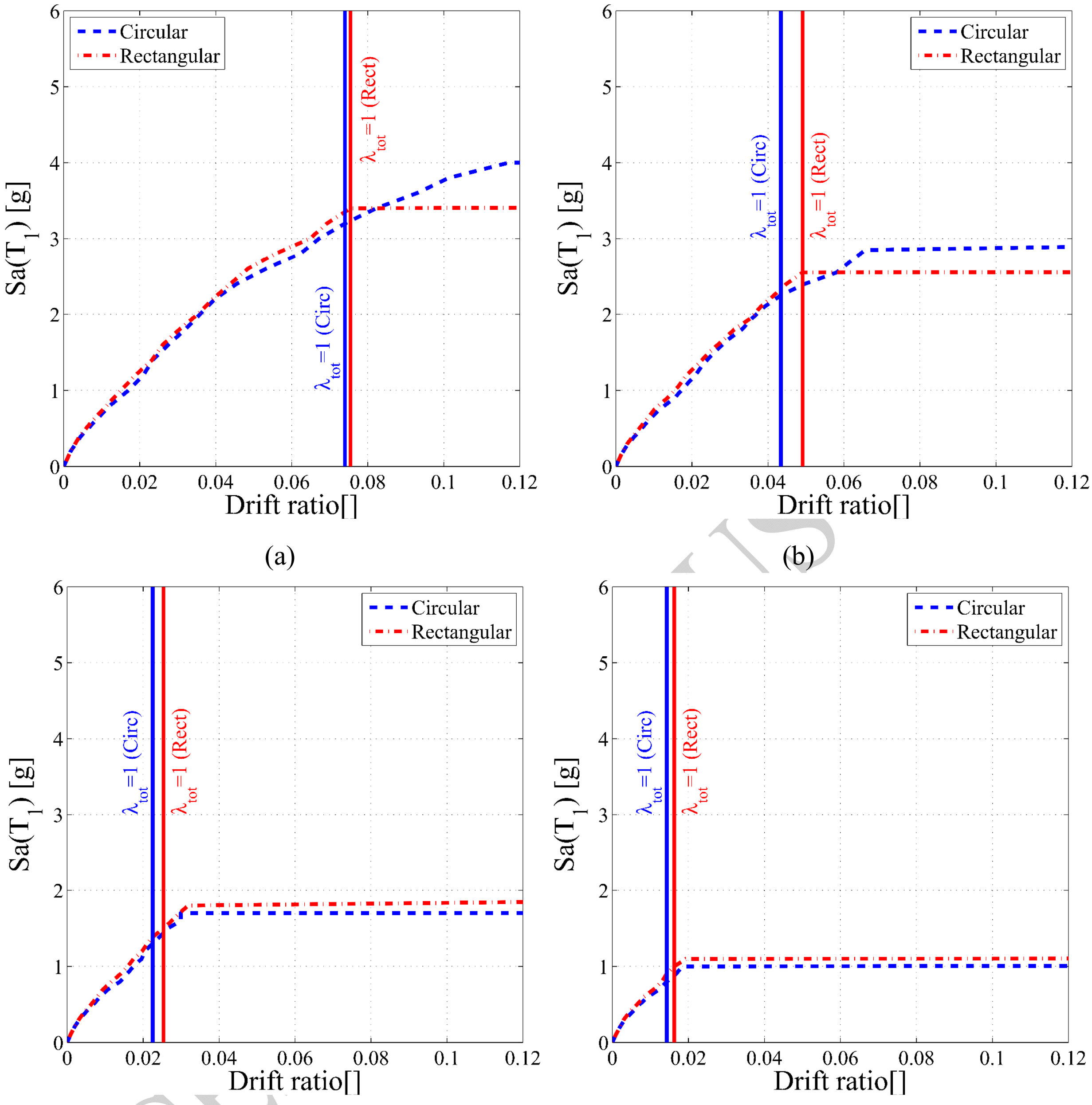

(a) (b)

(c) (d)

Fig. 12. Prediction of failure of median IDA curves using the proposed damage index: (a) uncorroded; (b) 5% corroded; (c) 10% corroded and (d) 20% corroded columns

7. Conclusions

In this research, the combined influence of cross-sectional shape and corrosion damage on failure mechanism of two identical RC columns, including a circular and a rectangular section, is investigated. Furthermore, the corrosion damaged limit states are considered by proposing a dimensionless combined local damage index. The nonlinear behaviour of the columns is simulated using an advanced nonlinear finite element modelling technique. Through a series of monotonic pushover and IDAs, the failure modes of the columns are studied at both global and material scales.

The main findings of the study can be summarised as follow:

- The severe corrosion changes the ductile behaviour of the columns, where the cover spalling occurs prior to yielding of the vertical bars.
- For lower corrosion levels, while the rectangular column collapses in a specified drift ratio and could not meet higher deformations, the circular column exhibits more ductile behaviour and fails gradually. This is attributed to the different pattern of core concrete crushing in circular section and rectangular section.
- While for lower corrosion levels, the failure mechanism of the circular column is core concrete crushing combined with fatigue failure of the reinforcements, for the higher corrosion levels its failure is dominated by core concrete crushing. However, for the different levels of corrosion, the failure of rectangular column is governed mainly by core concrete crushing.
- The proposed damage index accurately anticipates the failure of the rectangular columns with different levels of corrosion. It also relatively well predicts the failure of the 10% and 20% corroded circular columns. However, for the uncorroded and 5% corroded circular columns, the predicted failure point is somewhat earlier than their actual failure point.

References

Akiyama M, Frangopol DM, Matsuzaki H (2011) Life-cycle reliability of RC bridge piers under seismic and airborne chloride hazards. Earthquake Engineering and Structural Dynamics 40:1671–1687.

Alipour A, Shafei B, Shinozuka M (2011) Performance evaluation of deteriorating highway bridges located in high seismic areas. Journal of Bridge Engineering 6: 597-611.

Berry M, Parrish M, Eberhard M (2004) Performance database user's manual. PEER. Univ. of Calif. Berkeley, <www.ce.washington.edu/~peera1>.

Belletti B, Vecchi F (2018) Implementation of Steel Constitutive Model Including Buckling in ARC_CL 2.1 Crack Model. 5th International fib Congress. Melbourne, Australia.

Bertolini L, Elsener B, Pedeferri P, Polder RB (2004) Corrosion of steel in concrete: Prevention, diagnosis, repair. Weinheim: Wiley-VCH.

Coronelli D, Gambarova P (2004) Structural assessment of corroded reinforced concrete beams: modelling guidelines. J Struct Eng 130 (8): 1214-1224.

Cosenza E, Manfredi G (2000) Damage indices and damage measures. Progress in Structural Engineering and Materials 2(1):50–59.

Dhakal RP, Maekawa K (2002) Reinforcement stability and fracture of cover concrete in reinforced concrete members. Journal of Structural Engineering 128(10), 1253-1262.

Di Carlo F, Meda A, Rinaldi Z (2017) Numerical evaluation of the corrosion influence on the cyclic behaviour of RC columns. Engineering Structures, 53: 264-278.

Dizaj EA, Madandoust R, Kashani MM (2018a) Exploring the impact of chloride-induced corrosion on seismic damage limit states and residual capacity of reinforced concrete structures. Struct Infrastruct Eng 14(6):714–29.

Dizaj EA, Madandoust R, Kashani MM (2018b) Probabilistic seismic vulnerability analysis of corroded reinforced concrete frames including spatial variability of pitting corrosion. Soil Dynamics and Earthquake Engineering., 114: 97–112.

Du YG, Clark LA, Chan AHC (2005a) Residual capacity of corroded reinforcing bars. Magazine of Conc Res., 57 (3): 135–147.

Du YG, Clark LA, Chan AHC (2005b) Effect of corrosion on ductility of reinforcing bars. Magazine of Conc Res., 57 (7): 407–419.

Fang C, Lundgren K, Plos M, Gylltoft K (2006) Bond behaviour of corroded reinforcing steel bars in concrete. Cement Concrete Res, 36: 1931-1938.

FEMA P695 (2009) Quantification of Building Seismic Performance Factors. Federal Emergency Management Agency, Washington, DC.

Ghosh J, Padgett JE (2010) Aging considerations in the development of time-dependent seismic fragility curves. Journal of Structural Engineering., 136(12): 1497-1511.

Ghosh J, Sood P (2016) Consideration of time-Evolving capacity distributions and improved degradation models for seismic fragility assessment of aging highway bridges. Reliability Engineering & System Safety., 154: 197–218.

Guo A, Li H, Ba X, Guan X, Li H (2015b) Experimental investigation on the cyclic performance of reinforced concrete piers with chloride-induced corrosion in marine environment. Engineering Structures., 105: 1-11.

Guo A, Yuan W, Lan Ch, Guan X, Li H (2015a) Time-dependent seismic demand and fragility of deteriorating bridges for their residual service life. Bulletin of Earthquake Engineering., 13(8): 2389-2409.

Kappos AJ (1997) Seismic damage indices for RC buildings: evaluation of concepts and procedures. Progress in Structural Engineering and Materials., 1(1):78–87.

Karsan ID, Jirsa JO (1969) Behaviour of concrete under compressive loading. Journal of Structural Division., 95(ST12).

Kashani MM. (2014) Seismic Performance of Corroded RC Bridge Piers: Development of a Multi-Mechanical Nonlinear Fibre Beam-Column Model. PhD Thesis, Bristol: University of Bristol.

Kashani MM, Alagheband P, Khan R, Davis S (2015a) Impact of corrosion on low-cycle fatigue degradation of reinforcing bars with the effect of inelastic buckling. International Journal of Fatigue, 77, 174–185.

Kashani MM, Barmi AK, Malinova S (2015c) Influence of inelastic buckling on low-cycle fatigue degradation of reinforcing bars. Construction and Building Materials., 94, 644-655.

Kashani MM, Crewe AJ, Alexander NA (2017) Structural capacity assessment of corroded RC bridge piers. Proceedings of the Institution of Civil Engineers: Bridge Engineering, 170 (1): 28-41.

Kashani MM, Lowes LN, Crewe AJ, Alexander NA (2015b) Phenomenological hysteretic model for corroded reinforcing bars including inelastic buckling and low-cycle fatigue degradation. Comput Struct., 156: 58-71.

Kashani MM, Lowes LN, Crewe AJ, Alexander NA (2016) Nonlinear fibre element modelling of RC bridge piers considering inelastic buckling of reinforcement. Eng Struct., 116: 163-177.

Kashani MM, Maddocks J, Afsar Dizaj E (2019) Residual Capacity of Corroded Reinforced Concrete Bridge Components: A State-of-the-Art Review. Journal of Bridge Engineering., DOI: 10.1061/(ASCE)BE.1943-5592.0001429).

Kashani MM, Salami MR, Goda K, Alexander N (2018) Nonlinear flexural behaviour of RC columns including bar buckling and fatigue degradation. Magazine of Concrete Research., 70(5): 231-247.

Lehman DE, Moehle JP, Mahin SA, Calderone AC, Henry H (2004) Experimental Evaluation of Seismic Design Provisions for Circular Reinforced Concrete Columns. J of Struct Eng., 130 (6): 869-879.

Ma Y, Che Y, Gong J (2012) Behavior of corrosion damaged circular reinforced concrete columns under cyclic loading. Construction and Building Materials., 29: 548-556.

Mander JB, Priestley MJN, Park RJ (1988) Theoretical stress–strain model for confined concrete. Journal of Structural Engineering 114(8):1804–25.

Manson SS (1965) Fatigue: A complex subject-Some simple approximations. Exp Mech., 5 (7): 193–226.

McKenna F (2011) OpenSees: a framework for earthquake engineering simulation. Computing in Science & Engineering., 13(4): 58-66.

Meda A, Mostosi S, Rinaldi Z, Riva P (2014) Experimental evaluation of the corrosion influence on the cyclic behaviour of RC columns. Engineering Structures., 76: 112-123.

Mergos PE, Kappos AJ (2010) Seismic damage analysis including inelastic shear–flexure interaction. Bull Earthquake Eng., 8:27–46.

Mergos PE, Kappos AJ (2012) A gradual spread inelasticity model for R/C beam–columns, accounting for flexure, shear and anchorage slip. Engineering Structures., 44: 94-106.

Mergos PE, Kappos AJ (2013) A combined local damage index for seismic assessment of existing RC structures. Earthquake Engineering and Structural Dynamics, 42:833–852.

Mergos PE, Kappos AJ (2015) Estimating fixed-end rotations of reinforced concrete members at yielding and ultimate. Structural Concrete, 16(4), 537–545.

Ni Choine M, Kashani MM, Lowes LN, O'Connor A, Crewe AJ, Alexander NA (2016) Nonlinear dynamic analysis and seismic fragility assessment of a corrosion damaged integral bridge. International Journal of Structural Integrity., 7(2): 227-239.

Popovics S (1988) A numerical approach to the complete stress strain curve for concrete. Cement and Concrete Research., 3(5):583–99.

Priestley M, Paulay T (1992) Seismic design of reinforced concrete and masonry buildings. New York: John Wiley & Sons, Inc.

Rao AS, Lepech MD, Kiremidjian AS, Sun XY (2016a) Simplified structural deterioration model for reinforced concrete bridge piers under cyclic loading. Structure and Infrastructure Engineering., 13(1): 55–66.

Rodriguez ME (2015) Evaluation of a proposed damage index for a set of earthquakes. Earthquake Engineering and Structural Dynamics., 44:1255–1270.

Schneider J, Shen Y, Stiemer SF, Tesfamariam S (2015) Assessment and comparison of experimental and numerical model studies of cross-laminated timber mechanical connections under cyclic loading. Construction and Building Materials., 77: 197–212.

Scott BD, Park R, Priestley MJN (1982) Stress-strain behavior of concrete confined by overlapping hoops at low and high strain rates. ACI J 79 (1): 13-27.

Thanapol Y, Akiyama M, Frangopol DM (2016) Updating the Seismic Reliability of Existing RC Structures in a Marine Environment by Incorporating the Spatial Steel Corrosion Distribution: Application to Bridge Piers., Journal of Bridge Engineering., 21(7): 1-17.

Williamson SJ, Clark LA (2000) Pressure required to cause cover cracking of concrete due to reinforcement corrosion. Magazine of Conc Res 52 (6): 455-467.

Yuan W, Guo A, Li H (2017) Seismic failure mode of coastal bridge piers considering the effects of corrosion-induced damage. Soil Dynamics and Earthquake Engineering., 93:135-146.

Zhao J, Sritharan S (2007) Modeling of strain penetration effects in fiber-based analysis of reinforced concrete structures. ACI structural journal., 104(2): 133-141.